nature neuroscience

Functional organization for color and orientation in macaque V4

Hisashi Tanigawa[1], Haidong D Lu[1,2] & Anna W Roe[1]

Visual area V4 in the macaque monkey is a cortical area that is strongly involved in color and shape perception. However, fundamental questions about V4 are still debated. V4 was initially characterized as a color-processing area, but subsequent studies revealed that it contains a diverse complement of cells, including those with preference for color, orientation, disparity and higher-order feature preferences. This has led to disputes and uncertainty about the role of V4 in vision. Using intrinsic signal optical imaging methods in awake, behaving monkeys, we found that different feature preferences are functionally organized in V4. Optical images revealed that regions with preferential response to color were largely separate from orientation-selective regions. Our results help to resolve long-standing controversies regarding functional diversity and retinotopy in V4 and indicate the presence of spatially biased distribution of featural representation in V4 in the ventral visual pathway.

Neurophysiological and neuroanatomical evidence from the macaque monkey suggest that the cortical representation of different visual attributes, such as color (hue and luminance) and shape (contour orientation) features of visual objects, are preferentially localized in different compartments in early visual cortical areas (such as blobs and interblobs in the primary visual area V1 and thick, thin stripes and interstripes in the secondary visual area V2)[1,2]. Although this has led to a concept of functionally segregated streams in these early visual areas, there is also substantial evidence for merging and interaction between these streams[3–5]. Whether representation of these visual features remains localized in higher cortical areas is unknown.

V4 in the macaque monkey is a mid-tier cortical area in the ventral object-processing pathway that is strongly involved in color and shape perception. Given the prevalence of neurons that are selective for color, it was initially characterized as a color-processing area[6]. However, subsequent studies revealed that V4 contains not only color-selective cells, but also many cells selective for other features, including orientation[7–9]. However, no studies to date have addressed the organization of both color and orientation preference in V4 (ref. 10). To study the functional organization in V4 and address whether color and orientation representations are still localized to some degree in higher order areas, we examined the mapping of color and orientation preference in V4 of awake monkeys with optical imaging techniques. The existence of featural segregation in V4 would have important implications for studies on the role of V4 in visual perception and feature-based attention[11].

RESULTS

We used intrinsic signal optical imaging to reveal feature preference maps for color and orientation in dorsal V4 of macaque monkeys performing a fixation task. Imaging fields of view included a portion of V4 representing the central visual field (<7° eccentricity) and, in some cases, a portion of V2 along the lunate sulcus. Reflectance images under 630-nm illumination were acquired during presentation of isoluminant red/green grating patches (R/G) or achromatic luminance contrast grating patches (Lum), tilted 45° or 135° from the horizontal. The stimulus-evoked reflectance change from the pre-stimulus period was calculated pixel by pixel. The maps of reflectance change were spatially high-pass filtered to remove low spatial-frequency gradients, averaged across presentations in each stimulus condition and subtracted by the map obtained in the blank (no stimulus) condition to form single-condition maps (blank subtraction, see Online Methods). Typically, signal amplitudes in single-condition maps increased over the 3-s time course after the stimulus onset with peak magnitudes around −0.05 to −0.1% (note that a negative reflectance change indicates signal; **Fig. 1**), consistent with previous optical imaging studies[12,13]. Most sites exhibited some response to each stimulus. However, the signal intensity differed from site to site depending on stimulus condition (**Fig. 1a**). Some sites exhibited a larger change to either R/G (**Fig. 1b**) or Lum (**Fig. 1c**) stimuli and no orientation preference, whereas other sites were orientation selective (**Fig. 1d**,**e**) regardless of grating color type (R/G or Lum). Sites with selectivity for a particular combination of orientations and color types were also observed (**Fig. 1f**).

To reveal the spatial distribution of sensitivity to differences in stimulus features in foveal V4, we calculated difference maps between the single-condition maps in two imaging cases (case 1, ~0.75° eccentricity; **Fig. 2a**; case 3, ~1.5° eccentricity; **Fig. 2b**). In one case, the difference map of R/G minus Lum stimulus conditions showed several dark spots alternating with light spots along and anterior to the lunate sulcus (**Fig. 2c**), indicating clusters of pixels with greater response to either R/G or Lum. Using the same dataset, the difference map of 45° minus 135° stimulus conditions revealed a different set of dark and light spots, most of which were observed away from and anterior to

[1]Department of Psychology, Vanderbilt University, Nashville, Tennessee, USA. [2]Present address: Institute of Neuroscience, Chinese Academy of Sciences, Shanghai, China. Correspondence should be addressed to A.W.R. (anna.w.roe@vanderbilt.edu).

Received 21 July; accepted 28 September; published online 14 November 2010; doi:10.1038/nn.2676

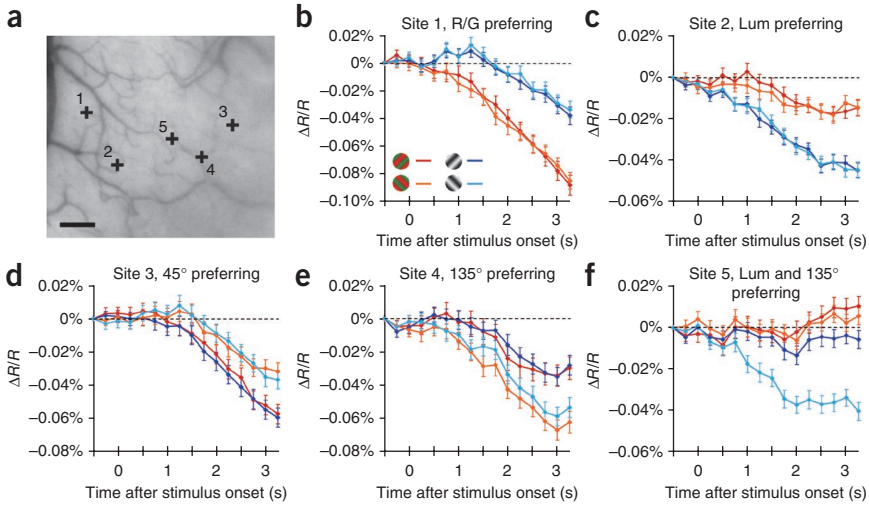

Figure 1 Examples of time course of stimulus-evoked reflectance change in V4. (**a**) Sampled sites indicated by black crosses on an image of exposed V4 cortical surface taken under 570-nm illumination. Scale bar represents 1 mm. (**b**–**f**) Time courses of average reflectance change ($\Delta R/R$) under 630-nm illumination at the sampled sites (160 μm in diameter) in response to a stimulus patch containing one of four types of gratings (red, 45° R/G; orange, 135° R/G; blue, 45° Lum; blue, 135° Lum; see Online Methods for details). The response values were taken from the single condition map, in which high-pass filtering and blank subtraction were applied. Error bars represent s.e.m.

the lunate sulcus (**Fig. 2d**), indicating clusters of pixels with preference to either 45° or 135°, respectively. In another case, the difference maps also revealed clusters of pixels with preference to color type near the lunate sulcus (**Fig. 2e**) and clusters of pixels with preference to orientation away from the lunate sulcus (**Fig. 2f**). The preference regions located in V2 in case 1 should be noted (posterior to the lunate; **Fig. 2c**,**d**). These color type–preferring regions and orientation-preferring regions likely correspond to thin stripe and thick/pale stripe locations, respectively[12,14].

To evaluate the significance of these stimulus preferences, we performed a two-tailed *t* test on a pixel-by-pixel basis. Because pixels on or near large vessels had a substantial trial-by-trial fluctuation in optical signals even in the blank condition, we excluded these pixels from the statistical analysis (**Fig. 2g**–**n**, see Online Methods). The statistical maps in response to R/G versus Lum clearly revealed R/G-preferring regions (**Fig. 2g**,**i**) and Lum-preferring regions (**Fig. 2g**,**i**), which appeared to alternate or interdigitate. Similarly, the statistical maps in response to 45° versus 135° (**Fig. 2h**,**j**) revealed 45°-preferring regions (**Fig. 2h**,**j**) and 135°-preferring regions (**Fig. 2h**,**j**), which were also arranged in an interdigitating manner. The distribution of these stimulus preferences was largely conserved in statistical maps of individual pair-wise comparison: orientation-matched R/G versus Lum and color-matched 45° versus 135° (**Supplementary Fig. 1**).

To examine the relative locations of the color-sensitive regions and orientation-sensitive regions, we computed a two-way ANOVA at

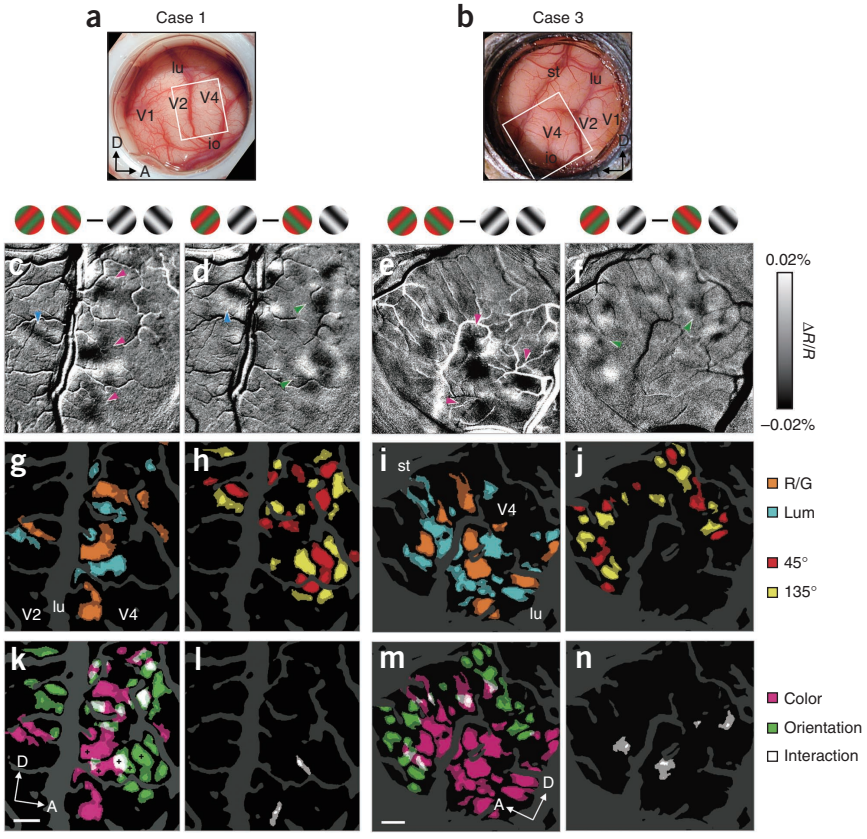

Figure 2 Functional maps of color and orientation sensitivity in foveal V4. (**a**,**b**) Views of the cortical surface including dorsal V4 through the imaging chamber. The white rectangles indicate the imaged regions (case 1, **a**; case 3, **b**). (**c**–**f**) Difference maps in response to R/G versus Lum (**c**,**e**) and 45° versus 135° (**d**,**f**). In these maps, dark versus light spots represent greater response to R/G versus Lum (**c**,**e**, magenta arrowheads) and 45° versus 135° (**d**,**f**, green arrowheads). Such spots were also observed in V2 (**c**,**d**, cyan arrowheads). Gratings above the maps indicate the subtraction pair for each difference map. (**g**–**j**) Statistical maps show significant differences in response to R/G versus Lum (**g**,**i**) and 45° versus 135° (**h**,**j**) (two-tailed *t* test, $n = 414$ trials for case 1 and 236 trials for case 3). Colored areas indicate significantly larger response to one of paired conditions, according to the key shown on the right. (**k**–**n**) Statistical maps created using two-way ANOVAs show regions with a significant main effect of stimulus color type (R/G versus Lum) (**k**,**m**, magenta), with a significant main effect of stimulus orientation (**k**,**m**, green) and with a significant interaction (**l**,**n**, white). In **g**–**n**, the brightness of color indicates the significance level, $P < 0.05$ (dark) and $P < 0.0001$ (bright), uncorrected, and dark gray regions indicate pixels with large cross-trial variability (Online Methods). The sampled sites in **Figure 1** are shown by black crosses in **k**. A, anterior; D, dorsal; io, inferior occipital sulcus; lu, lunate sulcus; st, superior temporal sulcus. Scale bar represents 1 mm (**c**–**n**).

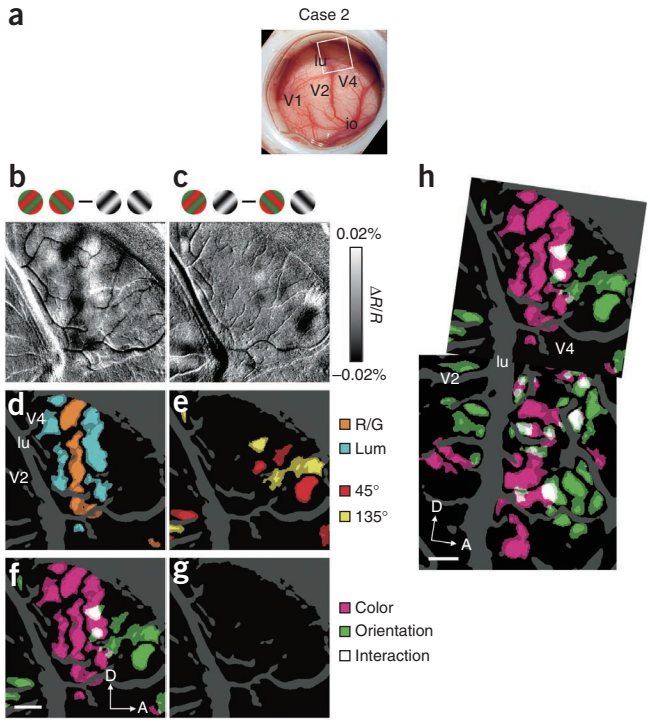

Figure 3 Functional maps of color and orientation sensitivity in parafoveal V4. (**a**–**g**) Data from a parafoveal V4 (~5° eccentricity) of the same animal as case 1 (case 2, $n = 400$ trials). Data are presented as in **Figure 2**. (**h**) Overlay of the maps of color-sensitive (magenta) and orientation-sensitive (green) regions in the foveal (**Fig. 2k**) and parafoveal V4 (**f**), aligned using the surface blood vessel pattern. Note the magenta and green regions in V2, consistent with thin and thick/pale stripe organization, respectively[12,14]. Scale bar represents 1 mm.

each pixel. One factor in the ANOVA was the stimulus color type (R/G versus Lum) and the other factor was the stimulus orientation (45° versus 135°). On the basis of the ANOVA, we visualized the color-sensitive regions (**Fig. 2k**,**m**) and orientation-sensitive regions (**Fig. 2k**,**m**), in which significant modulation ($P < 0.05$) was observed in either factor. This revealed that these color-sensitive and orientation-sensitive regions were largely segregated with some overlapping regions. The percentage of pixels falling in overlapping regions was only 5.90 ± 5.81% of the total area of regions with any significant modulation in each case (mean ± s.d., $n = 4$ imaging cases). The regions with a significant interaction between the two factors (color type and orientation; **Fig. 2l**,**n**) were rarely observed (2.68 ± 3.44%), indicating that distribution of these color- or orientation-sensitive regions was mostly independent.

The relative organization of these color-sensitive and orientation-sensitive regions differed between the two cases. In case 1, the color-sensitive regions were located posteriorly close to the lunate sulcus (**Fig. 2k**), whereas most of the orientation-sensitive regions were located about 2 mm away from the lunate sulcus (**Fig. 2k**). In case 3, the color-sensitive region (**Fig. 2m**) fell between the two band-like orientation-sensitive regions (**Fig. 2m**). The difference in the pattern of segregation between these two cases could be a result of differences in cortical eccentricity or of variability between animals. Despite these differences, these data indicate a clear segregation of domains concerned with color and with orientation in foveal V4.

Such segregation continued in the parafoveal portion of V4 (**Fig. 3**). We moved the field of view to a more dorsal location in the imaging chamber, a region representing ~5° eccentricity (case 2; **Fig. 3a**). Difference maps showed dark or light spots in this portion, revealing clusters of pixels with a modulation by either color (**Fig. 3b**) or orientation (**Fig. 3c**) change in the stimulus. Statistical maps for R/G versus Lum (**Fig. 3d**) and for 45° versus 135° (**Fig. 3e**), respectively, revealed color-preferring and orientation-preferring regions. Consistent with foveal imaging of case 1, there was an anterior-posterior segregation of color-sensitive and orientation-sensitive regions (**Fig. 3f**). In this case, there was no region with an interaction effect between stimulus color type and orientation in two-way ANOVAs (**Fig. 3g**). The continuity of this segregation is illustrated (**Fig. 3h**) by overlaying the maps from the foveal (**Fig. 2k**) and parafoveal V4 (**Fig. 3f**). These two types of feature-sensitive regions appear to fall in large band-like regions (also seen in case 3; **Fig. 2m**). We therefore refer to these color- and orientation-sensitive regions as color and orientation bands, respectively.

To further confirm the validity of these maps, we imaged V4 using a different set of color and orientation stimuli. In case 1, color and orientation bands were revealed by using gratings of four different colors and two different orientations with the same luminance profile (**Supplementary Fig. 2**). The color and orientation bands were distributed in a similar manner to the maps revealed by R/G and Lum imaging (**Fig. 2k**; see **Supplementary Table 1** for areal measurements of color and orientation bands). Although increasing stimulus variation revealed more overlap between color and orientation bands, the total area of these overlapping regions was smaller in all cases than that expected by chance (estimated by multiplying the percentage of color-sensitive pixels by that of the orientation-sensitive pixels). These results indicate that the observed cortical segregation of color versus orientation bands was robust regardless of which stimulus set used. Furthermore, the locations of these bands were invariant across different stimulus sizes (**Supplementary Fig. 3**).

The presence of apparently segregated functional regions in V4 raises the issue of relationship to retinotopy. Is there a single retinotopic map or multiple maps in this region? To explore this, we used a relatively small grating patch (1° in diameter) and presented it at different locations in the visual field (**Fig. 4**). As the stimulus location shifted away from the vertical meridian along a line of iso-eccentricity, in the color band, the activation shifted from posterior to anterior (**Fig. 4a**–**c**). In the orientation bands, the map shifted from the posterior band (**Fig. 4d**) to spanning both the anterior and posterior bands (**Fig. 4e**) to primarily the anterior band (**Fig. 4f**). As the location of the patch moved from central to peripheral along an iso-polar line, the overall modulation shifted from ventral to dorsal, both in the color band (**Fig. 4g**–**i**) and in the orientation bands (**Fig. 4j**–**l**). The general topography was consistent with and extended the general V4 retinotopic map[15]. Notably, for a single stimulus location, multiple zones of modulation were observed: one in a color band (**Fig. 4b**) and two others in adjacent orientation bands (**Fig. 4e**). This data was consistent with a continuous shifting of separate zones of activation in each of the color and orientation bands. Moreover, the observed 'jumping' from one orientation band to another as the stimulus shifted in the visual field closely parallels what is observed across functional stripes in V2 (ref. 16). Although our observation was limited only to this portion of V4, our finding suggests that V4 contains multiple, interleaved retinotopic maps, perhaps similar to those found across V2 stripes[16].

One previously noted aspect of orientation maps in areas V1 and the thick/pale stripes in V2 is the regular progression of orientation selectivity across cortical columns. Previous studies have identified both linear progressions[17] and those that occur in pinwheels[18].

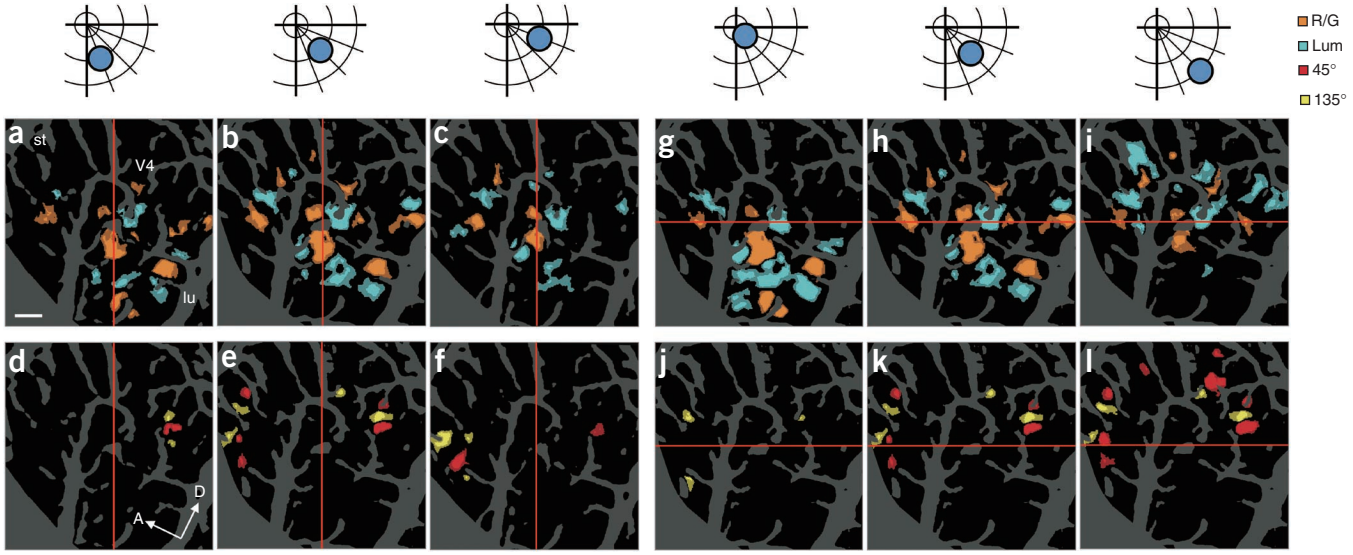

Figure 4 Overall spatial pattern of modulation by the stimulus at different locations in the visual field. (**a**–**f**) Response to shifting the polar angle. Regions with a significant difference in response to R/G versus Lum (**a**–**c**, case 3) and to 45° versus 135° (**d**–**f**), presented at a different polar angle with the same eccentricity as illustrated above (two-tailed *t* test, $n = 161$ (**a**,**d**), 159 (**b**,**e**) and 151 trials (**c**,**f**)). The center of stimuli was located at polar angles of 22.5° (**a**,**d**), 45° (**b**,**e**) and 67.5° (**c**,**f**) from the vertical meridian and an eccentricity of 1.5°. As the stimulus location moved away from the vertical meridian along a line of isoeccentricity, the overall activation shifted from posterior to anterior (use vertical red lines as guide). (**g**–**l**) Response to shifting the eccentricity. Regions with a significant difference in response to R/G versus Lum (**g**–**i**) and to 45° versus 135° (**j**–**l**), presented at a different eccentricity along an isopolar axis as illustrated above (two-tailed *t* test, $n = 164$ (**g**,**j**), 159 (**h**,**k**) and 159 trials (**i**,**l**)). The center of stimuli was located at a polar angle of 45° from the vertical meridian and at eccentricities of 0.5° (**g**,**j**), 1.5° (**h**,**k**) and 2.5° (**i**,**l**). As the stimulus location moved toward larger eccentricities, the overall activation shifted from ventral to dorsal (use horizontal red lines as guide). The size of grating patches was 1° in diameter. Scale bar represents 1 mm.

We examined whether such structures are also characteristic of orientation maps in V4 (**Fig. 5**). Difference maps from two imaging cases revealed orientation-selective regions as either dark or light spots (orientation domains; **Fig. 5a**,**b**,**d**,**e**). The size of orientation domains was 570 ± 120 μm in diameter (mean ± s.d., $n = 16$; see Methods for demarcation of the regions), larger than that in V2 (400 ± 100 μm, $n = 4$, two-tailed *t* test, $P = 0.025$). Corresponding color-coded polar maps of orientation preference with statistical significance (one-way ANOVA) were calculated (**Fig. 5c**,**f**). Examination of local regions in the maps revealed the presence of several pinwheel-like structures (**Fig. 5g**,**h**). We also found linear progressions of orientation preference in some cortical regions (**Fig. 5i**). Thus, not unlike V1 and V2, orientation-bands in V4 can contain both linear and pinwheel-like organizations for orientation.

Previous studies have demonstrated the presence of color maps in V1 blobs[19] and V2 thin stripes[12]. The presence of color maps in V4 has been postulated[6], but never demonstrated. A recent electrophysiological study revealed that neurons with similar color preferences are moderately clustered in V4 (ref. 20). To examine the presence of color maps in V4, we presented square-wave gratings with 100% luminance contrast either of six different hues or white (stimuli illustrated in **Fig. 6a**; see Online Methods for details). All colors including white had the same luminance. Some locations in V4 exhibited differential reflectance change in response to each hue

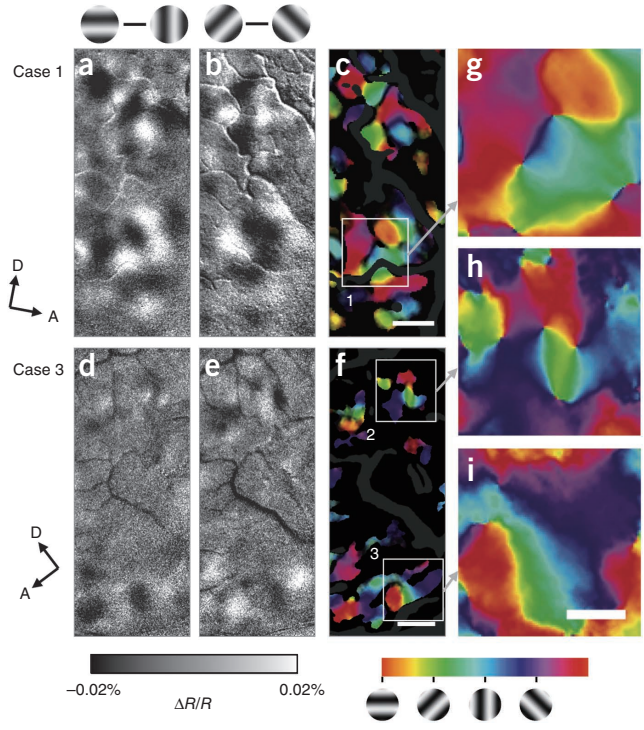

Figure 5 Functional maps of orientation preference in V4. (**a**,**b**) Difference maps to orthogonally oriented gratings (0°–90°, **a**; 45°–135°, **b**; case 1). Dark versus light pixels represent greater response to 0° versus 90° (**a**) and 45° versus 135° (**b**). (**c**) Color-coded polar map of orientation preference (orientation preference indicated by hue and magnitude of orientation selectivity by brightness. Pure black regions represent pixels without significant selectivity for orientation (ANOVA, 4 orientations, $P > 0.05$, uncorrected, $n = 690$ trials). (**d**–**f**) Data from another animal (case 3, $n = 468$ trials). Data are presented as in **a**–**c**. (**g**–**i**) Angle maps of regions in white frames in **c** and **f** (frame 1, **g**; frame 2, **h**; frame 3, **i**). In these maps, all hues are saturated in brightness to indicate only orientation preference. Scale bars represent 1 mm (**a**–**f**) and 0.5 mm (**g**–**i**).

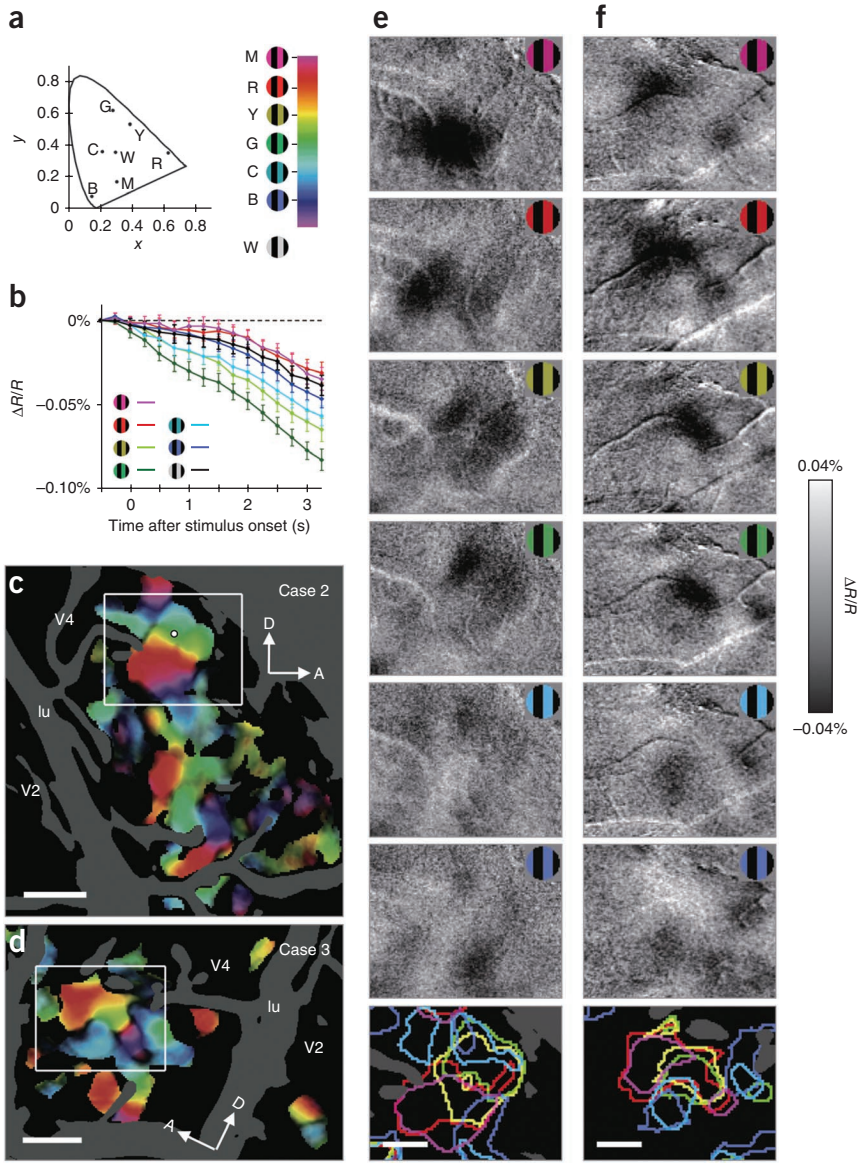

Figure 6 Functional map of hue preference in V4. (**a**) Left, stimulus colors plotted on the CIE 1931-*xy* chromaticity diagram (dots). M, magenta; R, red; Y, yellow; G, green; C, cyan; B, blue; W, white. Right, key for the hue-preference map. (**b**) Time courses of reflectance change at a sampled site (white dot in **c**) in response to each of six types of colored gratings and one type of achromatic gratings. Error bars represent s.e.m. Data are presented as in **Figure 1b**. (**c**,**d**) Large field views of color-coded polar maps of hue preference (case 2, **c**; case 3, **d**). Pixels with no significant selectivity for hue (one-way ANOVA, six hues, $P > 0.05$, uncorrected, $n = 707$ trials for **c**, $n = 495$ trials for **d**) and pixels with large cross-trial variability are shaded in black and dark gray, respectively. (**e**,**f**) Difference maps taken from the boxed region in **c** and **d**, respectively. These maps were calculated by subtracting the response to achromatic gratings from the response to each of six colored gratings (top to the second from the bottom). The regions with a significantly larger response to one of colored gratings than to achromatic gratings are outlined by that color in the bottom panels (two-tailed *t* test, $P < 0.05$ and peak $P < 0.0001$, uncorrected, $n = 231$, 230, 227, 229, 231 and 225 trials in **e**, $n = 165$, 170, 167, 162, 165 and 164 trials in **f**, from magenta to blue, respectively). Scale bars represent 1.0 mm (**c**,**d**) and 0.5 mm (**e**,**f**).

(**Fig. 6b**). We constructed color-coded polar maps of hue preference with statistical significance (one-way ANOVA) from the two cases (**Fig. 6c**,**d**). Not unlike orientation progressions, some hue progressions appeared to be more linear (**Fig. 6c**), whereas others appeared to be more circular (**Fig. 6d**), suggestive of hue-preference pinwheels. As illustrated by overlaying contours for R/G-preferring and Lum-preferring regions on these polar maps (**Supplementary Fig. 4**), R/G-preferring regions were located primarily in the hue-selective regions, particularly in the red/yellow/green-preferring domains. In contrast, Lum-preferring regions tended to include regions with low color preference and blue preference, similar to some previous reports of color preference in V2 (refs. 16,21). It is possible that blue-preferring domains would not have been activated by R/G gratings effectively and would have resided in Lum-preferring regions. Difference maps of hue-specific gratings minus achromatic gratings with the same contrast (**Fig. 6e**,**f**) showed dark spot(s) in response to the hue (hue domains). These dark spots shifted in location with changing hue. The size of hue domains was 600 ± 170 μm in diameter (mean ± s.d., $n = 17$), larger than that in V2 (370 ± 50 μm, $n = 4$, two-tailed *t* test, $P = 0.020$) and similar to the size of orientation domains.

To examine luminance invariance of the response of hue domains, we imaged hue domains in response to hue-specific gratings with different luminance levels (**Fig. 7**). In this imaging, we changed the luminance of colored strips in the gratings, but left the other components unchanged. We found that, in response to a specific hue, the same domains were activated across different luminance levels. This suggests that there are hue domains in V4 whose response is luminance invariant. This also indicates that the mapping of these hue domains was not a result of possible differences in isoluminance sensitivity between macaques and humans[22].

DISCUSSION

Using optical imaging techniques, we have revealed for the first time, to the best of our knowledge, the presence of spatially distinct distributions of orientation and color sensitivity in dorsal V4 of the macaque monkey. We found that, although most locations exhibit some activation to different stimuli, many locations exhibit preference for one stimulus over another. Not unlike ocular dominance segregation in V1 (where most cells are binocular), this provides evidence for at least some degree of cortical segregation of color and orientation representation in V4 (color and orientation bands). Our results are based on hemodynamic signals that reflect neuronal activity across a local population. This method is well suited for revealing local biases in representation at the columnar level, a level that is not easily detected by functional magnetic resonance imaging (fMRI) methods and, furthermore, may be missed by electrophysiological methods. It is important to emphasize that we do not suggest complete segregation of color and orientation representation at a cellular level

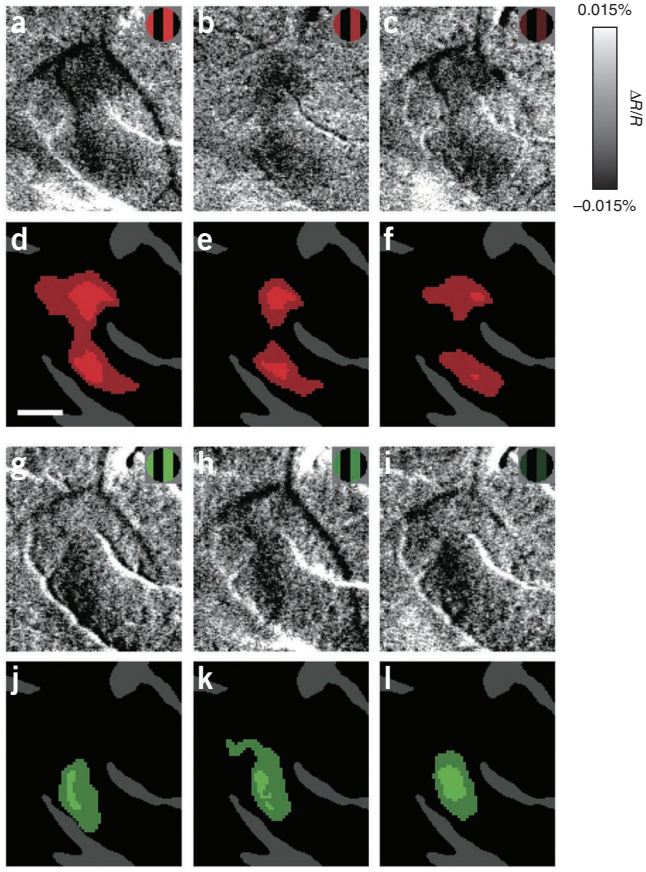

Figure 7 Luminance invariance in responses of hue-preferring region. (**a**–**c**) Difference maps of red/black gratings minus achromatic gratings (Lum) obtained from a color-responsive region of parafoveal V4 (case 4) with different luminance. The luminance of red strips in gratings used was 23.1 cd m^{-2} in **a**, 15.4 cd m^{-2} (33.3% darker) in **b** and 7.69 cd m^{-2} (66.7% darker) in **c**. The luminance of white strips in Lum and background was 23.1 cd m^{-2} and 11.6 cd m^{-2}, respectively. (**d**–**f**) Statistical maps show regions with a significantly larger response to red/black gratings than to Lum in **a**–**c** (colored areas, two-tailed *t* test, $n = 137$, 137 and 138 trials for **d**–**f**, respectively). (**g**–**i**) Difference maps of green/black gratings minus Lum obtained from the same region as in **a**–**c**. The luminance profiles of gratings were the same as in **a**–**c**, respectively. (**j**–**l**) Statistical maps show regions with a significantly larger response to green/black gratings than to Lum in **g**–**i** (two-tailed *t* test, $n = 105$, 103 and 104 trials for **j**–**l**, respectively). In the statistical maps (**d**–**f**,**j**–**l**), the brightness of color indicates the significance level, $P < 0.05$ (dark) and $P < 0.0001$ (bright), uncorrected, and dark gray regions indicate pixels with large cross-trial variability (Online Methods). Scale bar represents 0.5 mm.

in V4. The idea of cortical segregation of visual feature representation at early visual stages was originally proposed based on findings from anatomy and physiology[23]. However, many studies have shown that feature information is mixed at a cellular level and anatomical pathways are more intermingled than originally proposed[5]. It is likely that each of the color and orientation bands that we found in V4 includes some population of neurons responding to both types of visual feature or a mixture of neurons responding to either feature. However, on average, the local population response is biased toward features of color or of orientation selectivity.

We also suggest that these feature domains do not simply represent color and orientation. Given the known complex visual response properties in V4, such as selectivity for non-Cartesian (polar and hyperbolic) gratings[24], curved and angled contours[25], and combinations of color and shape[26], it is likely that these domains are regions of higher-order color and orientation processes. We speculate that the compartmentalization shown here may reflect a grouping of neurons processing complex visual features that share simple features as parts (for example, curved contours of opposite sign or different shapes with the same color).

Our findings help to clarify some of the controversies and confusion regarding V4. Early on, V4 was characterized as a color area, but this view was later modified as numerous studies failed to find a predominance of color cells. However, at least in the exposed foveal portion of V4, our data serve to revive an early electrophysiological report[27] that revealed a predominance of color-selective responses in the anterior bank of lunate sulcus (V4 proper), as compared with the prelunate gyrus (V4A). Recently, an fMRI study[28] found that there are several color-biased loci (globs) in the macaque cortex, one of which is located in the anterior bank of lunate sulcus. In addition, single-unit recording revealed that almost all cells recorded in these globs showed strong color tuning and orientation-sensitive cells were found more in the interglob[28]. This supports the presence of color and orientation bands in V4. Our findings are also consistent with those of neuroanatomical studies showing differential connectivity between anterior and posterior portions of V4 (refs. 29,30). However, the organization of color versus orientation representation in V4 might be more complex than simple subdivision along the anteroposterior axis. Some of our results (**Fig. 2m** and **Fig. 4**) suggest that V4 consists of multiple, alternating, band-like structures for color and orientation. Such band-like organization was also found in the pattern of afferent connections from V2 thin stripes and pale stripes[31]. In V3, it was demonstrated that there are two types of functional compartments: zones with high cytochrome-oxidase reactivity and high orientation selectivity and zones with low cytochrome-oxidase reactivity and low orientation selectivity[32]. Many of the disagreements regarding the areal boundaries, topography and functional focus of V4 (ref. 30) need to be reviewed given this new understanding regarding functional organization in V4.

Our data also support the presence of multiple retinotopic maps in V4. Stimuli located at single visual locations activate multiple foci in V4, which fall in both color and orientation bands, consistent with some previous suggestions regarding the presence of several retinotopic subdivisions in V4 (refs. 33,34). Thus, at a macroscopic scale, the visual field is represented smoothly in V4, as shown in electrophysiological mapping and fMRI studies[15,35]. However, at a finer scale, we propose that there are multiple, interleaved retinotopic maps and discontinuities in retinotopic progression between different functional compartments, similar to that previously described in V1 across ocular dominance columns[36] and in V2 across the thin, pale and thick stripes[16].

Why have past studies failed to observe these patterns of color- and orientation-sensitive regions in V4? Although difficult to visualize with the 2-deoxyglucose technique[37], some orientation-selective domains in V4 have been visualized in the foveal portion (<3°) of V4 by optical imaging in anesthetized monkeys[10]. With both 2-deoxyglucose technique[38] and with fMRI[28] methods, color-preferring cortical regions were observed across many visual areas. However, V4 activation in these studies was relatively weak. The difficulty in observing robust functional domain responses in V4 is perhaps a result of factors related to limitations of spatial resolution, anesthesia and/or the large size of full field stimuli, something that is likely to result in substantial surround suppression in V4 (ref. 39). Indeed, our own data reveal size-related attenuation of optical signal, particularly in color

response (**Supplementary Fig. 3**). Consistent with this, a more recent fMRI study[40], in which relatively small stimuli (6–10 degrees) were used, revealed abundant color-selective activation in macaque V4.

We predict that this study will affect studies of visual attention in V4 in two important ways. First, these images are obtained from the foveal region of V4. This region of V4 is an area that is virtually unstudied, despite the fact that in natural vision attention is almost always directed to the fovea. This approach thus opens the door on a new set of questions regarding the neural basis of foveal visual attention. Second, our results will strongly affect our thinking regarding the functional organizational basis of spatial and featural attention and, furthermore, the specificity of prefrontal influences on these organizations[41]. The ability to image functional organizations in higher visual areas of awake, behaving monkeys will make it possible to understand how functional domain activations are modulated by behavioral context (refs. 42,43; Tanigawa, H. & Roe, A.W., *Soc. Neurosci. Abstr.* **34**, 317.4, 2008).

METHODS

Methods and any associated references are available in the online version of the paper at http://www.nature.com/natureneuroscience/.

Note: Supplementary information is available on the Nature Neuroscience website.

ACKNOWLEDGMENTS

We thank J.H. Kaas and G. Chen for comments on the manuscript and Y. Chu for technical assistance. This work was supported by grants from the US National Institutes of Health, Vanderbilt Vision Research Center and Vanderbilt University Center for Integrative & Cognitive Neuroscience to A.W.R.

AUTHOR CONTRIBUTIONS

H.T. and A.W.R. designed the experiments. H.T. performed the experiments and analyzed the data. H.L. assisted H.T. with experimental procedures. H.T. and A.W.R. discussed the results and wrote the paper.

COMPETING FINANCIAL INTERESTS

The authors declare no competing financial interests.

Published online at http://www.nature.com/natureneuroscience/.
Reprints and permissions information is available online at http://www.nature.com/reprintsandpermissions/.

1. Livingstone, M.S. & Hubel, D.H. Anatomy and physiology of a color system in the primate visual cortex. *J. Neurosci.* **4**, 309–356 (1984).
2. Hubel, D.H. & Livingstone, M.S. Segregation of form, color, and stereopsis in primate area 18. *J. Neurosci.* **7**, 3378–3415 (1987).
3. Leventhal, A.G., Thompson, K.G., Liu, D., Zhou, Y. & Ault, S.J. Concomitant sensitivity to orientation, direction, and color of cells in layers 2, 3, and 4 of monkey striate cortex. *J. Neurosci.* **15**, 1808–1818 (1995).
4. Levitt, J.B., Kiper, D.C. & Movshon, J.A. Receptive field and functional architecture of macaque V2. *J. Neurophysiol.* **71**, 2517–2542 (1994).
5. Sincich, L.C. & Horton, J.C. The circuitry of V1 and V2: integration of color, form, and motion. *Annu. Rev. Neurosci.* **28**, 303–326 (2005).
6. Zeki, S.M. Colour coding in rhesus monkey prestriate cortex. *Brain Res.* **53**, 422–427 (1973).
7. Krüger, J. & Gouras, P. Spectral selectivity of cells and its dependence on slit length in monkey visual cortex. *J. Neurophysiol.* **43**, 1055–1069 (1980).
8. Schein, S.J., Marrocco, R.T. & de Monasterio, F.M. Is there a high concentration of color-selective cells in area V4 of monkey visual cortex? *J. Neurophysiol.* **47**, 193–213 (1982).
9. Tanaka, M., Weber, H. & Creutzfeldt, O.D. Visual properties and spatial distribution of neurones in the visual association area on the prelunate gyrus of the awake monkey. *Exp. Brain Res.* **65**, 11–37 (1986).
10. Ghose, G.M. & Ts'o, D.Y. Form processing modules in primate area V4. *J. Neurophysiol.* **77**, 2191–2196 (1997).
11. Maunsell, J.H. & Treue, S. Feature-based attention in visual cortex. *Trends Neurosci.* **29**, 317–322 (2006).
12. Xiao, Y., Wang, Y. & Felleman, D.J. A spatially organized representation of colour in macaque cortical area V2. *Nature* **421**, 535–539 (2003).
13. Vanzetta, I., Slovin, H., Omer, D.B. & Grinvald, A. Columnar resolution of blood volume and oximetry functional maps in the behaving monkey; implications for fMRI. *Neuron* **42**, 843–854 (2004).
14. Lu, H.D. & Roe, A.W. Functional organization of color domains in V1 and V2 of macaque monkey revealed by optical imaging. *Cereb. Cortex* **18**, 516–533 (2008).
15. Gattass, R., Sousa, A.P. & Gross, C.G. Visuotopic organization and extent of V3 and V4 of the macaque. *J. Neurosci.* **8**, 1831–1845 (1988).
16. Roe, A.W. & Ts'o, D.Y. Visual topography in primate V2: multiple representation across functional stripes. *J. Neurosci.* **15**, 3689–3715 (1995).
17. Hubel, D.H. & Wiesel, T.N. Sequence regularity and geometry of orientation columns in the monkey striate cortex. *J. Comp. Neurol.* **158**, 267–293 (1974).
18. Bonhoeffer, T. & Grinvald, A. Iso-orientation domains in cat visual cortex are arranged in pinwheel-like patterns. *Nature* **353**, 429–431 (1991).
19. Xiao, Y., Casti, A., Xiao, J. & Kaplan, E. Hue maps in primate striate cortex. *Neuroimage* **35**, 771–786 (2007).
20. Kotake, Y., Morimoto, H., Okazaki, Y., Fujita, I. & Tamura, H. Organization of color-selective neurons in macaque visual area V4. *J. Neurophysiol.* **102**, 15–27 (2009).
21. Wang, Y., Xiao, Y. & Felleman, D.J. V2 thin stripes contain spatially organized representations of achromatic luminance change. *Cereb. Cortex* **17**, 116–129 (2007).
22. Dobkins, K.R., Thiele, A. & Albright, T.D. Comparison of red-green equiluminance points in humans and macaques: evidence for different L:M cone ratios between species. *J. Opt. Soc. Am. A Opt. Image Sci. Vis.* **17**, 545–556 (2000).
23. Livingstone, M. & Hubel, D. Segregation of form, color, movement, and depth: anatomy, physiology, and perception. *Science* **240**, 740–749 (1988).
24. Gallant, J.L., Braun, J. & Van Essen, D.C. Selectivity for polar, hyperbolic and Cartesian gratings in macaque visual cortex. *Science* **259**, 100–103 (1993).
25. Pasupathy, A. & Connor, C.E. Responses to contour features in macaque area V4. *J. Neurophysiol.* **82**, 2490–2502 (1999).
26. Kobatake, E. & Tanaka, K. Neuronal selectivities to complex object features in the ventral visual pathway of the macaque cerebral cortex. *J. Neurophysiol.* **71**, 856–867 (1994).
27. Zeki, S. The distribution of wavelength and orientation selective cells in different areas of monkey visual cortex. *Proc. R. Soc. Lond. B Biol. Sci.* **217**, 449–470 (1983).
28. Conway, B.R., Moeller, S. & Tsao, D.Y. Specialized color modules in macaque extrastriate cortex. *Neuron* **56**, 560–573 (2007).
29. Zeki, S.M. Cortical projections from two prestriate areas in the monkey. *Brain Res.* **34**, 19–35 (1971).
30. Stepniewska, I., Collins, C.E. & Kaas, J.H. Reappraisal of DL/V4 boundaries based on connectivity patterns of dorsolateral visual cortex in macaques. *Cereb. Cortex* **15**, 809–822 (2005).
31. Xiao, Y., Zych, A. & Felleman, D.J. Segregation and convergence of functionally defined V2 thin stripe and interstripe compartment projections to area V4 of macaques. *Cereb. Cortex* **9**, 792–804 (1999).
32. Xu, X. *et al.* Functional organization of visual cortex in the owl monkey. *J. Neurosci.* **24**, 6237–6247 (2004).
33. Van Essen, D.C. & Zeki, S.M. The topographic organization of rhesus monkey prestriate cortex. *J. Physiol. (Lond.)* **277**, 193–226 (1978).
34. Maguire, W.M. & Baizer, J.S. Visuotopic organization of the prelunate gyrus in rhesus monkey. *J. Neurosci.* **4**, 1690–1704 (1984).
35. Fize, D. *et al.* The retinotopic organization of primate dorsal V4 and surrounding areas: a functional magnetic resonance imaging study in awake monkeys. *J. Neurosci.* **23**, 7395–7406 (2003).
36. Hubel, D.H. & Wiesel, T.N. Functional architecture of macaque monkey visual cortex. *Proc. R. Soc. Lond. B Biol. Sci.* **198**, 1–59 (1977).
37. Vanduffel, W., Tootell, R.B., Schoups, A.A. & Orban, G.A. The organization of orientation selectivity throughout macaque visual cortex. *Cereb. Cortex* **12**, 647–662 (2002).
38. Tootell, R.B., Nelissen, K., Vanduffel, W. & Orban, G.A. Search for color 'center(s)' in macaque visual cortex. *Cereb. Cortex* **14**, 353–363 (2004).
39. Desimone, R. & Schein, S.J. Visual properties of neurons in area V4 of the macaque: sensitivity to stimulus form. *J. Neurophysiol.* **57**, 835–868 (1987).
40. Harada, T. *et al.* Distribution of colour-selective activity in the monkey inferior temporal cortex revealed by functional magnetic resonance imaging. *Eur. J. Neurosci.* **30**, 1960–1970 (2009).
41. Moore, T. & Armstrong, K.M. Selective gating of visual signals by microstimulation of frontal cortex. *Nature* **421**, 370–373 (2003).
42. Hayden, B.Y. & Gallant, J.L. Time course of attention reveals different mechanisms for spatial and feature-based attention in area V4. *Neuron* **47**, 637–643 (2005).
43. Koida, K. & Komatsu, H. Effects of task demands on the responses of color-selective neurons in the inferior temporal cortex. *Nat. Neurosci.* **10**, 108–116 (2007).

ONLINE METHODS

All surgical and experimental procedures were approved by the Vanderbilt Animal Care and Use Committees and conformed to the guidelines of the US National Institutes of Health.

Animal preparation. The subjects in this experiment were two adult rhesus monkeys (*Macaca mulatta*, 5 and 8 kg, respectively). Prior to the imaging, under sterile surgical conditions, each monkey was anesthetized and implanted with a headpost and a chronic nylon imaging chamber overlying dorsal V4. Native dura in the chamber was replaced with a clear artificial dura (Tecoex, Thermedics Polymer Products). The chamber was sealed with a nylon cap and opened under sterile conditions for image acquisition. The chamber was located on the right hemisphere of one monkey (cases 1 and 2) and on the left hemisphere of another (cases 3 and 4). Retinotopic mapping experiments were performed using a spot or bar stimulus beforehand to examine whether our imaging regions were surely located in V4. In all cases, stimulus closer to the vertical meridian activated regions closer to the lunate sulcus, consistent with known retinotopy in V4 (ref. 15). The procedures for surgery, anesthesia and maintenance of chamber were previously described in detail[14,44].

Awake optical imaging. Monkeys were trained for juice reward to sit calmly with their heads fixed and to fixate a spot (0.15°) on a CRT monitor (xation window radius, < 0.75°). Eye position was monitored with an infrared eye tracker (RK-801, ISCAN, or iView X, SensoMotoric Instruments). Monkeys were required to maintain fixation throughout each image acquisition (4 s). The detailed imaging methods have been described previously[14,44]. Under 630-nm illumination, images of light reflectance from V4 cortex were captured (4 s per trial) through a CCD video camera (504 × 504 pixels, 8 × 8 mm; 1M60P, Dalsa) with a tandem lens system focused on the cortical surface, and digitized by Imager 3001 (12-bit resolution, 4 frames per second, Optical Imaging). Image acquisition included a 0.5-s prestimulus period, followed by 3.5-s stimulus presentation period. Each experiment contained 4–16 stimulus conditions and one blank condition (no stimulus except fixation point); each condition was repeated 40–100 times, pseudo-randomly interleaved with at least a 1.5-s intertrial interval. This means that the interstimulus interval was 2.0 s, including the 0.5-s prestimulus period (see **Supplementary Note** and **Supplementary Figs. 5** and **6** for the validity of this intertrial interval). Only trials with successful fixation throughout were further analyzed. The success rate was 88.5 ± 3.7% (mean ± s.d., $n = 7$ imaging sessions).

Visual stimuli. Visual stimuli were created using VSG 2/5 or ViSaGe (Cambridge Research Systems) and presented on the CRT monitor that was gamma corrected using a photometer (Minolta Chroma Meter CS-100, Ramsey) and positioned 118 or 140 cm from the eyes. To examine color, luminance and orientation preference in V4, we presented a circular patch filled with isoluminant red/green or luminance-contrast (100%) black/white drifting sinusoidal gratings (1–2 cycles per degree, 0.5–1° s^{-1} drift rate, two orthogonal orientations) on a uniform gray background. Drifting direction was randomized on every trial. Gratings had an average luminance of 26.8 cd m^{-2}, identical to the background luminance.

To study color preference, we used patches of color/black drifting square-wave gratings with 100% luminance contrast (2 cycles per degree spatial frequency, 1° s^{-1} drift rate, two orthogonal orientations). We used six different hues and one white with CIE-*xy* chromaticity coordinates (0.63, 0.34, red; 0.39, 0.53, yellow; 0.28, 0.61, green; 0.22, 0.35, cyan; 0.15, 0.07, blue; 0.31, 0.16, magenta; 0.30, 0.33, white; **Fig. 6a**). All colors including white had the same luminance (11.5 cd m^{-2}) and the average luminance of gratings was the same as the background luminance (5.75 cd m^{-2}). In all cases, the size and location of patches were optimized to stimulate the imaged region. In case 1, 2, 3 and 4, the size was 1°, 4°, 1.5° and 4° in diameter, and the center was located at 0.75°, 6°, 1.5° and 4° eccentricity, respectively, unless otherwise specified.

Data analysis. Images in trials with successful fixation throughout were used. Image frames were analyzed offline using custom software (MATLAB, Mathworks). All images were first corrected for any brain movements (induced by animal movements), by aligning each frame to the first frame using blood vessels as landmarks. For each trial, frames between 1 and 3.5 s after the stimulus onset were averaged, and then subtracted and divided by the frame 0.5 s before the onset on a pixel-by-pixel basis to obtain maps of reflectance change ($\Delta R/R$ map). To remove nonstimulus-specific global signal changes and reveal local modulation, each $\Delta R/R$ map was convolved with a 1.6 × 1.6-mm median filter and subtracted from the original maps (high-pass filtering, see **Supplementary Fig. 7**). Finally, all filtered $\Delta R/R$ maps obtained in one stimulus condition were averaged to form the single condition map. Difference maps between two stimulus conditions were obtained by calculating the average difference of filtered $\Delta R/R$ maps between the conditions.

We used a two-tailed *t* test for a comparison of the response between two stimulus conditions and a one-way ANOVA to evaluate a response modulation caused by the difference in one feature dimension (orientation or hue). The *P* value was calculated at each pixel in filtered $\Delta R/R$ maps by either *t* test or ANOVA (*P* value map), uncorrected for multiple comparisons. In the *P* value maps, only regions that consisted of pixels with $P < 0.05$ and peak $P < 0.0001$ were regarded as being regions of significant modulation and regions that did not meet this criteria were excluded. We did not apply any correction for multiple comparisons to our *P* values in the maps. When the number of statistical comparisons conducted increases, the chance of a false-positive result also increases[45]. To estimate the likelihood of false-positive modulation expected by chance in our imaging method, we compared two sets of filtered $\Delta R/R$ maps obtained during odd- and even-numbered trials in the blank condition by a two-tailed *t* test. In all cases, no significant modulation was revealed by this comparison, indicating that it is unlikely that the observed significant modulations occurred by chance. Color-coded angle and polar maps of orientation-preference and hue-preference were created by pixel-wise vectorial summation of single condition maps of four different orientations or six different hues, respectively[46]. To remove high-spatial-frequency noise from the *P* value, angle and polar maps, we smoothed each $\Delta R/R$ map before analysis by using a 240 × 240-μm mean filter.

Signals from pixels on and near large vessels were less reliable because of large trial-by-trial fluctuation[47], something that occurred even without visual stimulation. To exclude these regions from the analysis, we calculated pixel-wise s.d. of blank condition images across trials. Pixels with large s.d. (>the upper limit of 95% one-sided confidence interval based on the χ^2 distribution) were eliminated from further analysis (shaded in gray in the *P* value and polar maps). To measure the size of orientation-selective and hue-selective activation regions, we compared single-condition maps with the average 'cocktail blank' response to all examined orientations and hues, respectively, using two-tailed *t* test. Regions that consisted of pixels with $P < 0.05$ and peak $P < 0.0001$ were regarded as being stimulus-specific local activations. The diameter of each activation region was measured by averaging its length (the diameter along the long axis) and width (the diameter along the short axis) with ImageJ (US National Institutes of Health).

44. Chen, L.M. *et al*. A chamber and artificial dura method for long-term optical imaging in the monkey. *J. Neurosci. Methods* **113**, 41–49 (2002).
45. Huettel, S.A., Song, A.W. & McCarthy, G. *Functional Magnetic Resonance Imaging* (Sinauer Associates, Sunderland, Massachusetts, 2004).
46. Bonhoeffer, T. & Grinvald, A. Optical imaging based on intrinsic signals: the methodology. in *Brain Mapping: the Methods* (eds. Toga, A.W. & Mazziotta, J.C.) 55–97 (Academic Press, New York, 1996).
47. Zhan, C.A. & Baker, C.L. Jr. Boundary cue invariance in cortical orientation maps. *Cereb. Cortex* **16**, 896–906 (2006).